

## Research Article

# Automated Scoring to Assess RAD51-Mediated Homologous Recombination in Ovarian Patient-Derived Tumor Organoids

Lucie Thorel<sup>a,b,\*</sup>, Nicolas Elie<sup>c</sup>, Pierre-Marie Morice<sup>a,b</sup>, Louis-Bastien Weiswald<sup>a,b,d</sup>,  
Romane Florent<sup>d</sup>, Marion Perréard<sup>a</sup>, Florence Giffard<sup>a,b,c</sup>, Agathe Ricou<sup>e,f</sup>, Raphaël Leman<sup>e,f</sup>,  
Guillaume Babin<sup>g</sup>, Jean-François Lebrun<sup>g</sup>, Sandrine Martin<sup>g</sup>, Mélanie Briand<sup>a,b,h</sup>,  
Bernard Lambert<sup>a</sup>, Florence Joly<sup>a,i</sup>, Cécile Blanc-Fournier<sup>a,h,j</sup>, Dominique Vaur<sup>e,f</sup>,  
Enora Dolivet<sup>a,g</sup>, Benoit Plancoulaine<sup>a,b,k</sup>, Laurent Poulain<sup>a,b,d,h,\*</sup>

<sup>a</sup> INSERM U1086 ANTICIPE, Université de Caen Normandie, Caen, France; <sup>b</sup> Comprehensive Cancer Center François Baclesse, UNICANCER, Caen, France; <sup>c</sup> US PLATON-VIRTUAL'HIS Platform, Université de Caen Normandie, Caen, France; <sup>d</sup> US PLATON- ORGAPRED core facility, Université de Caen Normandie, Caen, France; <sup>e</sup> Department of Cancer Biology and Genetics, Comprehensive Cancer Center François Baclesse, UNICANCER, Caen, France; <sup>f</sup> INSERM U1245, Cancer Brain and Genomics, FHU G4 Génomique, Normandie Université, Rouen, France; <sup>g</sup> Department of Surgery, Comprehensive Cancer Center François Baclesse, UNICANCER, Caen, France; <sup>h</sup> US PLATON, UNICANCER, Biological Resource Center 'OvaRessources,' Comprehensive Cancer Center François Baclesse, Université de Caen Normandie, Caen, France; <sup>i</sup> Clinical Research Department, Comprehensive Cancer Center François Baclesse, UNICANCER, Caen, France; <sup>j</sup> Department of Biopathology, Comprehensive Cancer Center François Baclesse, UNICANCER, Caen, France; <sup>k</sup> Department of Pathology, Forensic Medicine and Pharmacology, Faculty of Medicine, Institute of Biomedical Sciences, Vilnius University, Vilnius, Lithuania

## ARTICLE INFO

## Article history:

Received 23 July 2024  
Revised 10 January 2025  
Accepted 13 January 2025  
Available online 23 January 2025

## Keywords:

functional assay  
homologous recombination  
ovarian cancer  
patient-derived tumor organoids

## ABSTRACT

Poly(ADP-ribose) polymerase inhibitors (PARPi) have been shown to improve progression-free survival, particularly in homologous recombination-deficient ovarian cancers. Identifying patients eligible for PARPi is currently based on next-generation sequencing, but the persistence of genomic scars in tumors after restoration of homologous recombination (HR) or epigenetic changes can be a limitation. Functional assays could thus be used to improve this profiling and faithfully identify homologous recombination-deficient tumors. The repair capacity (RECAP) test assesses the formation of RAD51 foci in proliferating cells after irradiation and can be used on tumors as well as on patient-derived tumor organoids (PDTO). However, RAD51 foci scoring is often performed manually without standardization. The purpose of this translational study was to develop an automated tool for scoring RAD51-mediated HR based on whole slide imaging of ovarian PDTO. To that end, we quantified Cyclin A2 and RAD51 immunofluorescence on 9 PDTO models derived from 8 ovarian cancer patients, and next, we compared the RECAP test results to genome instability score and to the patient clinical response. We therefore developed a standardized and automatized quantitative histomaging tool allowing a comparative RAD51 foci evaluation and thus to define the HR status in PDTO. Our RECAP-based classification was correlated to the genome instability score, offering a new opportunity for standardization of HR assessment in PDTO. This new automated tool to score HR status, which remains to be validated on a large cohort of patients, may thus be used as a

These authors contributed equally: Lucie Thorel, Nicolas Elie, Pierre-Marie Morice, Benoit Plancoulaine, and Laurent Poulain

\* Corresponding authors.

E-mail addresses: [L.POULAIN@baclesse.unicancer.fr](mailto:L.POULAIN@baclesse.unicancer.fr) (L. Poulain), [lucie.thorel@unicaen.fr](mailto:lucie.thorel@unicaen.fr) (L. Thorel).



complement to next-generation sequencing-based tests in order to improve the identification of the number of patients eligible for PARPi.

© 2025 THE AUTHORS. Published by Elsevier Inc. on behalf of the United States & Canadian Academy of Pathology. This is an open access article under the CC BY license (<http://creativecommons.org/licenses/by/4.0/>).

## Introduction

The integrated genomic analyses conducted by The Cancer Genome Atlas Research Network in 2011 led to a better understanding of the complex molecular aberrations of epithelial ovarian carcinomas.<sup>1</sup> Molecular analyses of tumors showed that up to 50% exhibit alterations of the homologous recombination (HR) pathway. This error-free DNA repair mechanism maintains the integrity and stability of the genome in order to avoid cell death via central core proteins such as ataxia telangiectasia mutated (ATM), BRCA, and RAD51. HR defects lead to the accumulation of double-strand breaks (DSB) in DNA and broken or stalled replication forks.<sup>2</sup> To exploit this homologous recombination deficiency (HRD), poly(ADP-ribose) polymerase inhibitors (PARPi) have been used with a synthetic lethality approach.<sup>3,4</sup> PARP enzymes are known to repair single-strand breaks, and their inhibition, when combined with HRD, induces further lethal DSB, which is highly tumor-specific and not adequately repaired.<sup>5,6</sup>

Extensive trials of PARPi have shown that they improve progression-free survival in patients with ovarian cancers.<sup>7-9</sup> This improvement applies particularly to patients carrying germline and somatic *BRCA1/2* mutations and in HRD subgroups. In a large study including many cancer types, Alexandrov et al.<sup>10</sup> identified, in 2013, multiple distinct mutational signatures including the single-based substitution signature 3 (SBS3) and the small insertion and deletion signature 5 (ID6), both associated with HRD status. However, to date, identifying patients eligible for PARPi has been a challenge for scientific and clinical teams using next-generation sequencing (NGS) analysis. NGS-based selection identifies genomic alterations (eg, *BRCA* mutations), genomic instability (eg, loss of heterozygosity), or genomic signature (eg, HRD status) by using labeled companion diagnostic tests as well as specific gene panels. However, the persistence of genomic scars in tumors after restoration of proficient HR or epigenetic changes is a limitation of NGS, and the same applies to gene aberrations depending on the test used (commercial vs homemade).<sup>11-13</sup> To improve the profiling of HR status, some authors have used functional tests that faithfully identify HRD tumors.<sup>14</sup> For example, the repair capacity (RECAP) test assesses the formation of RAD51 foci in proliferating cells after ex vivo irradiation of fresh primary breast cancer tissue.<sup>15,16</sup> The RECAP test and its derivatives have also been performed on tumor-derived organoids.<sup>17</sup> These tools have predictive value in the context of personalized medicine as they directly assess the response to treatments and the functionality of DNA repair pathways. However, RAD51 foci scoring is often performed manually without any possibility of the standardization of techniques. By contrast, recent progress in whole slide imaging (WSI), referring to scanning a complete microscope slide and creating a single high-resolution digital file, could represent an opportunity for automatizing the evaluation of HR. The purpose of this translational study was to develop an automated tool for scoring RAD51-mediated HR to assess tumor heterogeneity. We used the tool on ovarian cancer tumor-derived organoids and compared the result to the genome instability

determined by the genome instability score (GIS) companion diagnostic test (GIScar).<sup>13</sup>

## Materials and Methods

### Tumor Samples

#### Ethical Considerations

Fresh tumoral tissue and ascitic fluids (n = 9) from ovarian cancers were collected from patients treated at the Comprehensive Cancer Center François Baclesse (Unicancer Center, Normandy). Informed consent forms were signed by all patients and were obtained either by the Biological Resources Center "OvaResources," which has received NF 96 900 accreditation (N° 2016/72860.1) or in the context of the "OVAREX" clinical trial (N°ID-RCB: 2018-A02152-53, NCT03831230), in accordance with ethical committee and European law. Clinical, treatment, and histopathologic details were extracted from patient charts. A medical pathologist (C.B.-F.) analyzed all samples.

#### Next-Generation Sequencing of Patient Samples

DNA from paraffin-embedded tumor samples was extracted with a Qiacube automate (Qiagen) using QIAamp DNA formalin-fixed paraffin-embedded (FFPE) kits. Tumor DNA was sequenced with a panel of 22 HR-related genes, enabling the identification of *BRCA1/2* mutations. Agilent SureDesign (Agilent) was used to create library baits covering the exonic regions of these genes. Regions of interest were captured using the SureSelect XT Protocol (Agilent) and sequenced on Illumina NextSeq (Illumina) using the paired-end 2×75bp program. Bioinformatic analysis was performed with BclToFastq 2.20 (Illumina) for demultiplexing, followed by BWA 0.7.12 for alignment and the GATK v3.8 pipeline to produce BAM files, according to the Broad Institute recommendations. The variant-calling step was carried out by HaplotypeCaller, Lofreq v2.1.1, and outLyzer v2. Only single nucleotide variants and Indels with an allele ratio greater than 1% were analyzed. Variants identified were annotated with Alamut Batch 1.7.0 (Interactive Biosoftware) and Annovar, and the results were plotted on Excel sheets (Microsoft Office).

#### Genomic Instability Scoring of Patient-Derived Tumor Organoid

In order to assess PDTO HR status, PDTOs were sequenced with a 127-gene panel including 15 HR genes (*BRCA1*, *BRCA2*, *ATM*, *BARD1*, *BRIP1*, *CDK12*, *CHEK1*, *CHEK2*, *FANCL*, *PALB2*, *PPP2R2A*, *RAD51B*, *RAD51C*, *RAD51D*, and *RAD54L*). The sequencing data were then used to determine a genomic instability score (GIS) as described by Leman et al.<sup>13</sup> Briefly, this genomic instability score was based on a first analysis by a CNVkit pipeline v0.9.7.<sup>18</sup> From the CNVkit data outcomes, 3 scores of instability were calculated: the number of large genomic events, the structural instability score, and the allelic imbalance. Then, these scores were used in the logistic model to compute a mathematic Esperance that the tumor is HR-proficient (HRP) or HRD, with a value tending to 0 for HRP tumors and a value tending to 1 for HRD tumors. The decision-making threshold

between HRP and HRD tumors was 0.48. However, this threshold was defined on FFPE tumor tissue, and at the time of this work, we could not propose an optimal threshold for PDTO. Thus, we defined a third category HRDmid corresponding to PDTO with a score at more and less than 0.25 the threshold of FFPE tumor tissues (0.48), that is, a range score of 0.23 to 0.73.

### *Patient-Derived Tumor Organoids*

#### *Processing of Samples*

Tumor tissue was cut into 4 mm<sup>3</sup> pieces. One piece was fixed in 3% paraformaldehyde for paraffin inclusion and histopathological/immunohistochemistry analyses, and another piece was processed to establish organoids. Tumor sample dissociation was performed using the Tumor Dissociation human kit and a gentleMACS Dissociator (Miltenyi Biotec). Sterile tumor ascitic samples were centrifuged (2000 rpm for 5 minutes). Pellets containing cells were resuspended in 20 mL of Roswell Park Memorial Institute 1640 medium (Fisher Scientific) supplemented with 10 IU/mL penicillin, 10 µg/mL streptomycin (Fisher Scientific), and 1% bovine serum albumin (BSA) (Sigma). Suspensions were strained successively in 300 µm and 50 µm filters (Endcotts). The remaining cells or spheroids were digested in 2 mL of TrypLE Express (Fisher Scientific) at 37 °C for 30 to 60 minutes.

Dissociated cells were collected in organoid basal medium (OBM: Advanced DMEM [Fisher Scientific], 10 IU/mL penicillin, 10 µg/mL streptomycin, 1% GlutaMAX-1 [Fisher Scientific]) and pelleted (2000 rpm for 5 minutes). Additionally, 10,000 cells were resuspended in organoid culture medium (OBM supplemented with B27 [Fischer Scientific, 200 µL/mL], N-Acetyl-L-cysteine [Sigma, 1.25 mM], epidermal growth factor [Miltenyi, 50 ng/mL], FGF-10 [Peprotech, 20 ng/mL], FGF-basic [Miltenyi, 1 ng/mL], A-83-01 [Peprotech, 500 nM], Y27632 [Selleckchem, 10 µM], SB202190 [Peprotech, 1 µM], Nicotinamide [Sigma, 10 mM], PGE2 [Sigma, 1 µM], Primocin [InvivoGen, 100 µg/mL], cultrex HA-R-Spondin-1-Fc 293T [AMS Bio, 50% V/V], and Cultrex L-WRN [AMS Bio, 10% V/V], mixed with Cultrex Reduced Growth Factor Basement Membrane Extract, Type 2 on a 1:1 ratio) and seeded in a prewarmed 24-well plate (Eppendorf). After polymerization (37 °C, 5% CO<sub>2</sub>, 15 minutes), each drop was immersed in 500 µL of organoid culture medium. The medium was exchanged twice a week as needed for the duration of the culture. Once harvested with OBM supplemented with 1% BSA (OBM-BSA), organoids were dissociated using TrypLE Express (37 °C for 30-60 minutes). Isolated cells were seeded or biobanked (Coolcell, -80 °C) in 500 µL of recovery cell culture freezing medium (Fisher Scientific) for future use.

#### *Patient-Derived Tumor Organoid Culture*

When organoids measured around 75 to 150 µm, they were collected using cold OBM-BSA, centrifuged at 200 g for 2 minutes, and incubated with TrypLE Express for up to 15 minutes at 37 °C. After dissociation, the cells were centrifuged at 430 g for 5 minutes, suspended in organoid culture medium, counted, and plated at 10,000 cells per 50 µL drop of 1:1 Basement Membrane Extract, Type 2/cell suspension in prewarmed 24-well plates. The plates were transferred to a humidified 37 °C/5% CO<sub>2</sub> incubator. Cryovials were prepared at regular intervals by dissociating and resuspending organoids in recovery cell culture freezing medium (Gibco), then placed in a cell freezing container (Coolcell) at -80 °C and biobanked at -150 °C on the next day. PDTO lines were authenticated by comparison of their short tandem repeat profiles with that of the tumor of origin (Microsynth).

### *Histology and Immunohistochemistry*

Tissue and PDTO were fixed in 3% paraformaldehyde overnight, embedded in 2% agarose, dehydrated, paraffin-embedded, and sectioned before standard hematein eosin saffron staining. Automated immunohistochemistry using a Ventana Discovery Ultra was performed on 4 µm-thick paraffin sections. Slides were deparaffinized with EZPrep buffer, and epitopes were unmasked by 15 minutes of high-temperature treatment in CC1 EDTA buffer. Sections were incubated for 40 minutes at 37 °C with an anti PAX8 (ab191870, Abcam, 1/500) and p53 (ab16665, Abcam, 1/100). Secondary antibody (Omnimap Rabbit HRP; Ventana Medical System Inc) was incubated for 16 minutes at room temperature. Immunodetection performed without the primary antibody was used as a control. After washes, the staining was performed with 3, 3'-diaminobenzidine, and the sections were counterstained with hematoxylin using Ventana reagents according to the manufacturer's protocol. Stained slides were then digitized using an Aperio ScanScope slide scanner (Aperio Technologies).

#### *Patient-Derived Tumor Organoid Irradiation*

To evaluate the HR status, we used the RECAP test described by Naipal et al.<sup>15</sup> On the day of irradiation, the medium of 6-well plates was collected and conserved at 37 °C, and 2 mL of OBM was added to each well (including the control plate) during the irradiation. The organoids were irradiated at 5 Gy (X-Ray [XR] source, 130 kV, 5 mA) in a CellRad X-irradiation system. After irradiation, the medium was discarded and replaced by the previously conserved warm organoid culture medium. After incubation of the plates for 2, 6, or 24 hours, the organoids were collected, washed with OBM-BSA, and fixed in 3% paraformaldehyde for at least 3 hours at +4 °C. Paraformaldehyde was then discarded, and the pellet was embedded in agarose, dehydrated, and paraffin-embedded (Autostainer XL, Leica).

#### *Patient-Derived Tumor Organoid Staining*

Immunofluorescence staining of RAD51 (ab133534, Abcam), γH2AX (ab11174, Abcam), and Cyclin A2 (ab211736, Abcam) was done on 4 µm sections of PDTO (microtome Leica) with the Ventana Discovery Ultra. Microscope slides with PDTO sections were deparaffinized with EZPrep buffer and the antigenic sites were unmasked with EDTA. The endogen peroxidase inhibitor (Roche) was used to limit background noise. Hundred microliters of previously diluted primary antibody (Primary Antibody Diluent, Clinisciences) were added to each slide and incubated at 37 °C for 40 minutes (1/100,000 for RAD51, 1/500,000 for γH2AX and 1/1000 for Cyclin A2). Then, after washing, the second antibody (Omnimap Rabbit) was incubated at 37 °C for 16 minutes. Finally, the DISCOVERY Rhodamin (Roche) and the DISCOVERY FITC (Roche) were added for RAD51 and Cyclin A2, respectively. The slides were subsequently stained for DAPI (Roche). At the end of the procedure, the slides were washed with detergent to eliminate the LCS oil layer and were hydrophilic-mounted with Fluoromount-G (CliniSciences). The slides were protected from light until digital acquisition.

#### *Digital Acquisition and Analysis*

##### *Imaging Settings*

Specimens of PDTO sections were digitized with an Olympus VS120 scanner equipped with a 40× objective (N.A 0.95), a light emitting diode illumination (Lumencor Spectra X 7 light emitting diode), a single multiband filter DAPI (emission: 455 nm; exposure time: 5 ms), FITC (518 nm; 20 ms), and CY3 (565 nm; 10 ms) filters

from Olympus and a CMOS camera from Hamamatsu (Orca Flash 4.0). Whole slide images were recorded with Extended Focal Imaging technology applied over a height of 4  $\mu\text{m}$  (Z-range) and an acquisition of 5 slices per field (0.84  $\mu\text{m}$  Z-spacing).

#### Quantification Processing

On each slide, the PDT0 were isolated automatically by detection using the Qupath program and the extension Cellpose.<sup>19,20</sup> For each individual organoid, nuclei detection was assessed on the DAPI channel, and the surface occupied by nuclei was processed—thanks to the extension StarDist on Qupath program.<sup>21</sup> For the positive nuclei detection Cyclin A2, 2 Gaussian filters of different sizes were applied on the FITC channel. Only the positive pixels obtained after the difference between the 2 filtered images were kept to obtain a binary image with the positive Cyclin A2 areas. Then, a geodesic reconstruction was applied between the images of nuclei and Cyclin A2 to identify only positive nuclei with a Cyclin A2 active. Finally, for the detection of RAD51 foci, the CY3 channel was used. RAD51 foci were detected—thanks to a Laplacian filter after a Gaussian operation, in the scikit-image python library.<sup>22,23</sup> Only bright foci on dark backgrounds are detected. For each nucleus of each organoid, only the RAD51 foci inside the CyA2-positive nuclei were kept and computed.

#### Gaussian Mixture Model Approach

A Gaussian Mixture Model<sup>24</sup> was used to determine the minimum threshold of RAD51 foci in proliferative cells (Cyclin A2-positive nuclei), making it possible to differentiate the basal level of HR DNA repair from irradiation-induced HR DNA repair. Ultimately, 1 Gaussian function was found, but it allowed the smoothing of the histograms.

#### Principal Component Analysis

Principal component analysis (PCA) was applied to keep only principal components (PC) or “new explanatory parameters” with maximum variance.<sup>25</sup> New PCA coordinates were defined by considering these selected PC, and then, the explained variables (as PDT0 models) were put in PCA space usually limited to 2 or 3 dimensions in order to have possibilities to find a better relationship between them. These PCA coordinates were computed by using the base-change matrix previously determined. Coordinates of the current or added later explained variables (as PDT0 models) were computed, therefore, by easy linear combination.

## Results

#### Patient and Tumor Characteristics

Overall, 9 women with stages III to IV ovarian cancer according to the International Federation of Gynecology and Obstetrics system were included in this study, 8 patients were diagnosed with a high-grade serous ovarian cancer, and 1 patient had a carcinosarcoma. According to pathologist analyses, PDT0s retained the histologic/immunohistochemical features of parental tumors (Supplementary Fig. S1).

With the exception of 1 patient with a BRCA2 pathogenic mutation (OV-156\_A), these tumors did not exhibit deleterious or suspected deleterious BRCA alterations or other potential mutations related to the HR status according to the

22 genes panel tested, but 2 patients undergone an additional HR testing during their clinical management using the Myriad Genetics MyChoice CDx signature and OV-196\_T came out as HRP, whereas OV-122\_T came out as HRD (Supplementary Table S1).

#### Homologous Recombination Evaluation Using Repair Capacity Test

To evaluate RAD51-mediated homologous recombination, we used 10 established PDT0 models presented in Supplementary Table S1. We induced single- and DSB in DNA using X-ray irradiation (5 Gy) and incubated them 2 to 24 hours postirradiation.  $\gamma\text{H2AX}$  staining to confirm XR-induced DNA damages is presented in Supplementary Figure S2. Then, we performed immunodetection of both RAD51, in order to identify HR foci, and Cyclin A2 in order to quantify the RAD51 foci only in cells in S/G2 phases. Indeed, we observed that cyclin A2 staining offered a better and cleaner signal than geminin, a frequently used stain in other studies, and that no or little discrepancies were observed between these 2 markers in PDT0 (data not shown). Representative colabeling observed before and after irradiation is shown in Figure 1.

As expected, RAD51 foci were mainly present in the nuclei of Cyclin A2-positive cells (Fig. 1A). Three types of profiles were observed: in the first one, the level of RAD51 foci was low both before and after irradiation (Fig. 1A, left panel), in the second one, the level was high both before and after irradiation (Fig. 1A, middle panel), and in the last and most common one, the RAD51 foci number increased after irradiation (Fig. 1A, right panel). This staining was automatically detected and quantified (Fig. 1B). Isolated PDT0 was detected automatically with the Cellpose method, and the Stardist method was used to individualize nuclei. Among them, Cyclin A2-positive cells were identified as described above, and RAD51 foci were also isolated and quantified in the nuclei of each proliferative cell.

Overall, 8,075 individualized PDT0 from 40 slides were detected automatically. The number of PDT0 detected in a single condition ranged from 14 to 557 with a median of 183 PDT0, and the number of Cyclin A2-positive nuclei for each condition ranged from 17 to 3,729, with a median of 308 (Supplementary Table S2). The high disparity in the number of PDT0 analyzed is due to disparities in PDT0 density in the paraffin-embedded pellets. However, this automated method makes it possible to analyze a much larger number of nuclei and PDT0 than manual quantification.

We first compared the distribution of the count of RAD51 foci in the Cyclin A2-positive cells before and 2, 6, or 24 hours after irradiation in all PDT0 models (Fig. 2A). This analysis showed that the distribution of RAD51 foci was heterogeneous between the models, both before and after irradiation. Indeed, the mean number of RAD51 foci was 7.2 foci per proliferative cell at baseline but with a standard deviation of 7.9.

In some cases, only slight modifications of this number occur over time after irradiation, whereas in other cases, a strong increase occurs after irradiation (mainly after 2 and 6 hours) before coming back or not to the baseline level after 24 hours.

Usually, a threshold value of 5 RAD51 foci per nucleus is used to distinguish HRP samples from HRD ones.<sup>15</sup> However, as the detection was automatized, the sensitivity of RAD51 foci detection was greatly increased. Indeed, because the mean number of RAD51 foci in control Cyclin A2-positive cells was 7.2, a threshold of 5 foci cannot be used to distinguish control cells from irradiated cells. To establish the threshold to be used

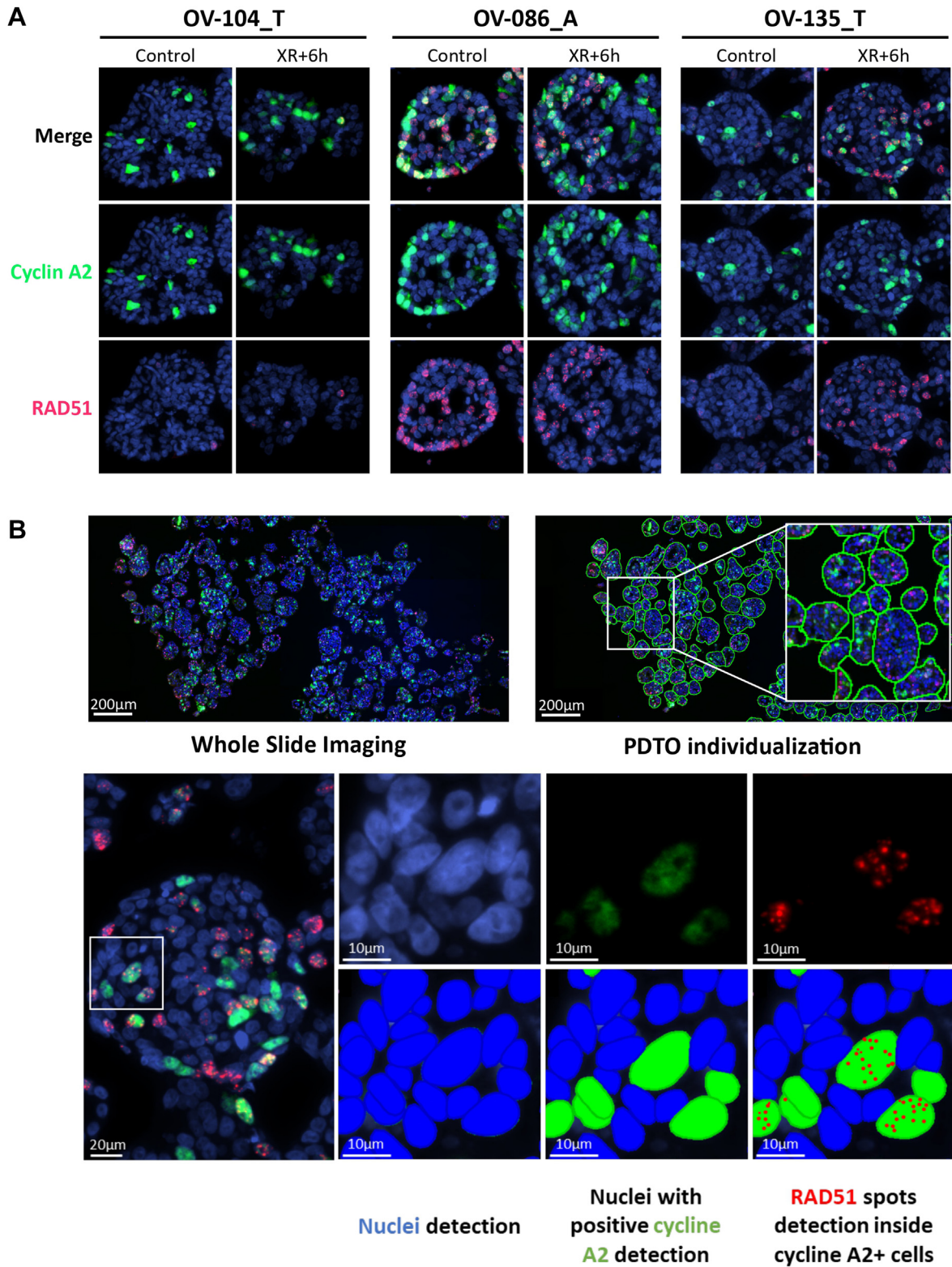


**Figure 1.**

Data acquisition and analysis. (A) PDTO coimmunostaining of nucleus (blue), Cyclin A2 (green), and RAD51 protein (red) before (control) and after X-ray irradiation (XR + 6 h). (B) PDTO individualization and automated quantification of RAD51 foci in cyclin A2-positive nuclei on the OV-135\_T model. PDTO, patient-derived tumor organoids; XR, X-ray.

for further analyses without using an a priori assumption, we used a Gaussian model approach. For each distribution obtained by pooling all data (RAD51 foci numbers in proliferative

cells) from all PDTO models for each condition, we found a Gaussian representing more than 60% of the overall population (range: 61%-85%).

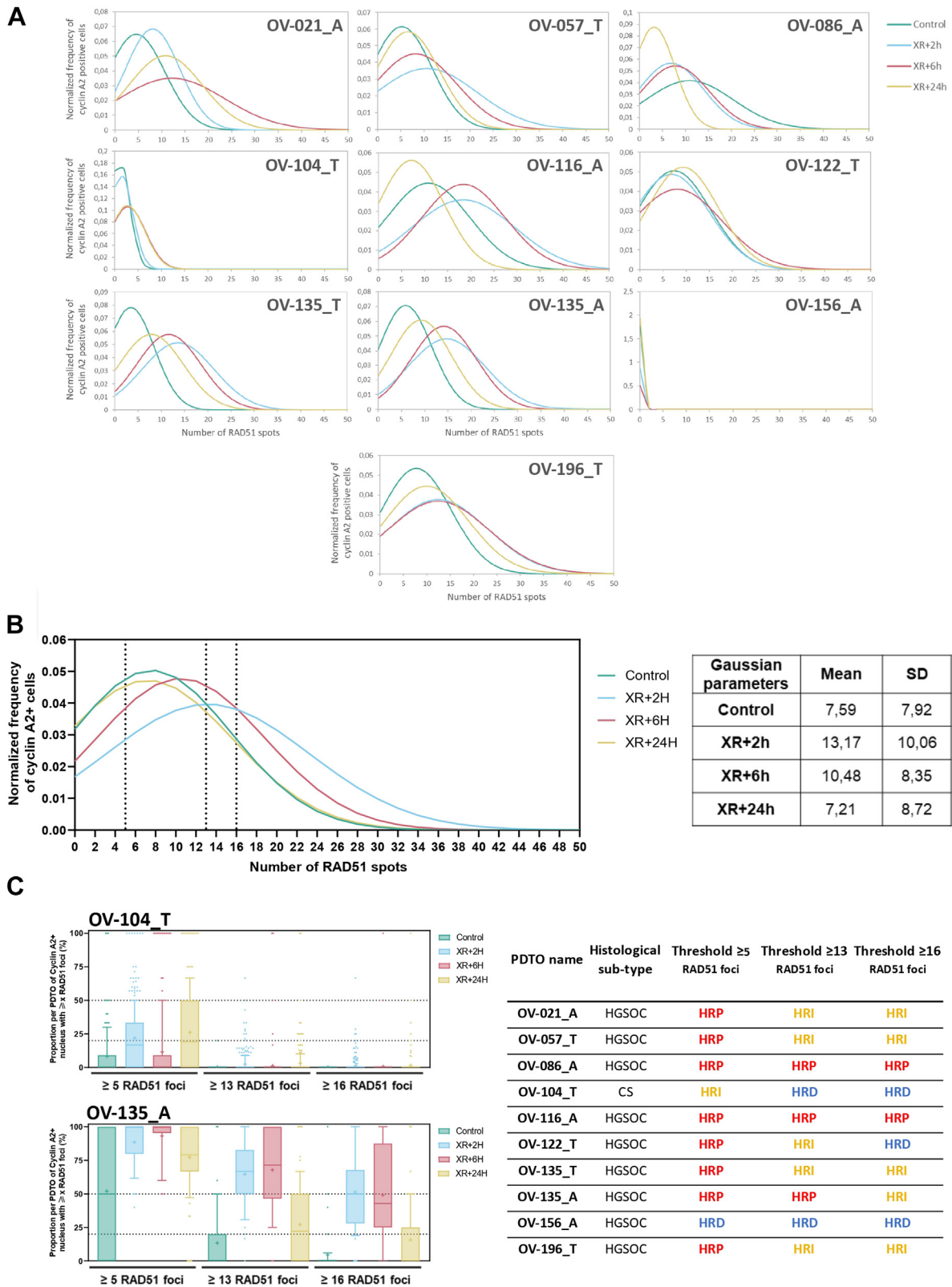
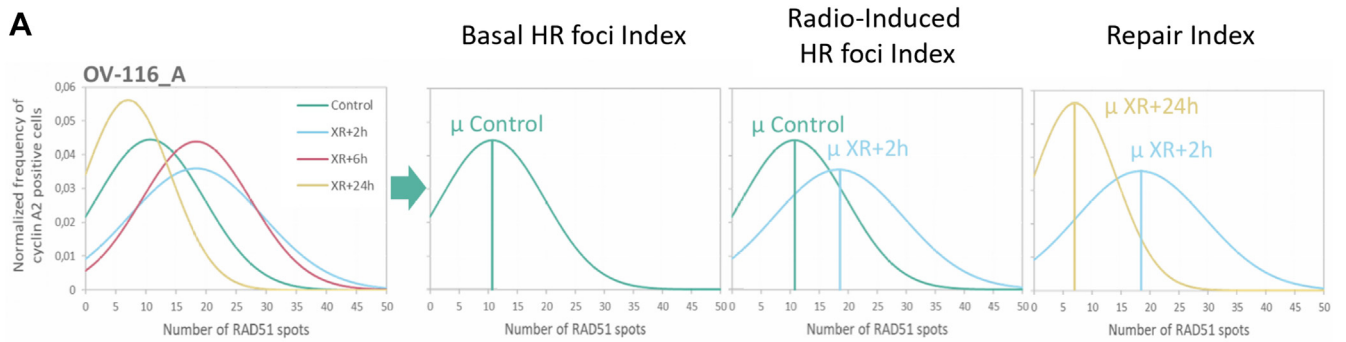


**Figure 2.**

Variation of RAD51 foci number following PDTO irradiation. (A) Gaussian functions of pooled data from 10 patient-derived tumor organoids (PDTO) models before (control) and after irradiation (XR + 2 h, XR + 6 h, and XR + 24 h). (B) Merge of the Gaussian functions and summary of Gaussian-associated descriptive data (mean and standard deviation [SD]). (C) Application of 3 different thresholds (5, 13, and 16 RAD51 foci) to the OV-104\_T and OV-135\_A PDTO models (right panel) and comparison of the HR classification on the 10 PDTO models depending on the threshold used (left panel). HR, homologous recombination; XR, X-ray.



**B**

PDTO name	Basal HR foci Index	Radio-Induced HR foci Index	Repair Index
OV-021_A	4,5	3,5	-2,8
OV-057_T	5,2	5,4	4,1
OV-086_A	10,9	-4,0	3,7
OV-104_T	1,0	0,3	-1,4
OV-116_A	10,8	7,6	11,3
OV-122_T	7,3	-0,6	-2,5
OV-135_T	3,4	10,2	5,8
OV-135_A	5,9	8,8	5,5
OV-156_A	1,5	0,7	0,7
OV-196_T	5,0	4,7	2,5

**Figure 3.**

Interpretation of RECAP test results based on 3 index scores. (A) Extrapolation of 3 indexes score: the basal HR foci index equals to the mean of the control Gaussian, the radio-Induced HR foci index equals to the difference between the mean of the control Gaussian and the mean of the XR + 2 h Gaussian and the repair index equals the difference between the mean of the XR + 2 h Gaussian and the mean of the XR + 24 h Gaussian. (B) Indexes are computed for each patient-derived tumor organoids model. HR, homologous recombination; RECAP, repair capacity; XR, X-ray.

Interestingly, the control and XR + 24 h Gaussian were close to each other, XR + 2 h Gaussian was the most distant from the control one, and XR + 6 h was intermediate, showing a progressive repair of DNA damages.

Using the comparison of the Gaussian from each condition (Fig. 2B), we defined that the mean value of the XR + 2 h RAD51 foci number was around 13 and that the intersection at 16 of the Gaussian XR + 2 h with the XR + 6 h Gaussian clearly distinguish them from XR + 24 h and control Gaussians (Fig. 2B). We thus used the value of 5, 13, and 16 RAD51 foci as thresholds for further analyses of the proportion per PDTO of Cyclin A2-positive nuclei with a number of RAD51 foci equal or superior to the chosen thresholds.

Results detailed in Figure 2C and in Supplementary Figure S3 showed that the interpretation when done using the Meijer et al.<sup>16</sup> thresholds of 50% and 20% clearly depends on the choice of the threshold and could lead to opposite or difficult conclusions. For example, a threshold of 5 RAD51 foci per Cyclin A2-positive cell classified the OV-104\_T model as HR-intermediate, whereas a threshold of 13 foci or 16 foci classified it as HRD. For another PDTO line OV-135\_A, a threshold of 5 and 13

RAD51 foci classified it as HRP, whereas a threshold of 16 classified it as HR-intermediate (Fig. 2C).

In order to better characterize the RECAP of each PDTO model without establishing a threshold that could impede inter-PDTO heterogeneity, 3 different indexes were described using the Gaussian approach (Fig. 3A). First, the basal HR foci index represents the basal amount of damage in each PDTO model and is equal to the mean of the control Gaussian. Second, the radio-induced HR foci index represents the amount of additional damage that result from the irradiation and is the difference between the mean of the 2 hours Gaussian and the mean of the control Gaussian. Finally, the repair index aims to characterize the effective repairation performed by the PDTO over time and is the difference between the mean of the 24 hours Gaussian and the mean of the 2 hours Gaussian. The basal HR foci index showed the heterogeneity of the basal amount of damage for each PDTO model, ranging from 3.4 to 10.9. The radio-induced HR foci index explained the amplitude of the X-ray-induced damage and ranged from -4 to 10.2. Finally, the repair index carried the effective repairation information and was ranging from -2.8 to 11.3 (Fig. 3B).

### Homologous Recombination Status Using Genomic Instability Score

The genome instability score was determined based on DNA extracted from each PDO model. An HRP model is characterized by a more stable variation of the copy ratio for all chromosomes (Fig. 4A, left panel), whereas an HRD profile will display a high instability (Fig. 4A, right panel). Of the 10 PDO models analyzed, 6 were classified as HRP, 3 as HRDmid, and 1 as HRD (Supplementary Fig. 4).

### Homologous Recombination Scoring: Repair Capacity Test Versus Genomic Instability

PCA of the newly described indexes (Fig. 3A and B) placed a group of 5 of our PDO models on the opposite side of all the other models when using the threshold 0 on the PC1 axe (Fig. 4B), allowing the discrimination of 2 groups that could correspond to HRD and HRP models. We thus compared this classification with the genome instability GIScar scoring and found that except for 1 case, OV-122\_T, 9 the 10 models presented the same phenotype (HRD or HRP) with these 2 analyses methods (Fig. 4B). We next performed a comparison of these classifications with the patient platinum-free interval (PFI) and showed that the misclassified case was the patient with the longest PFI (indicative of the sensitivity to platinum-based regimen), suggesting that the RECAP test identified an HRD status that was not captured by the GIScar scoring (Fig. 4C).

## Discussion

In order to allow a fast and reliable quantification of RAD51 foci in Cyclin A2-positive cells defining the HR DNA repair pathway in PDO from ovarian cancers, we have developed an operator-independent automatized tool. Each cell and organoid were considered separately in order to assess the degree of heterogeneity of HR status between cells and/or organoids in each PDO model. Moreover, we compared HR status between the models and compared the RECAP test with an academic GIScar and with the patient PFI.

All models exhibited a significant basal level of RAD51 foci in proliferative cells. RAD51 is a key component of the replication-associated DNA damage repair pathway and is particularly involved in the replication stress response.<sup>26</sup> Moreover, tumors that overexpress RAD51, including ovarian cancers, often exhibit an increased rate of HR, a more aggressive cancer phenotype, and resistance to treatment.<sup>27</sup> This phenomenon has also been reported in a breast cancer patient-derived xenograft model.<sup>28</sup> Surprisingly, Castroviejo-Bermejo et al.<sup>29</sup> also showed in some germline BRCA-mutated patient-derived xenograft that more than 20% of RAD51 cells were positive at baseline. Moreover, recent studies also described the presence of RAD51 foci in ovarian cancer cells at the basal level and established a link between the level of RAD51 foci and ovarian cancer patients' progression-free survival, using quantitative analysis.<sup>30</sup> The literature thus showed that the baseline level of RAD51 foci is sometimes difficult to interpret on its own and that the formation of irradiation-induced RAD51 foci could be highly informative for determining HR status. In this context, our study indeed showed that the analysis of RAD51 level after irradiation provides complementary information about the capacity of cells to not only engage HR DNA repair but also to efficiently repair the lesions.

Indeed, X-ray irradiation induced a significant increase in the number of RAD51 foci in the nuclei of proliferative cells, as already described by Naipal and Meijer.<sup>15,16</sup> However, in our case, both the increase and return to basal level varied in a PDO model-dependent manner. This kinetic analysis allowed us to define a basal HR foci index as well as a radio-induced HR foci index and a repair index, which are not possible to define without the irradiation step.

In our study, only 1 BRCA mutation was found (OV-156\_A), and no other HR-related mutation from the 22 gene panel was found in the 8 other patient tumor samples. Only 2 patients were tested by the Myriad MyChoice test during their clinical management among which 1 patient tumor was classified as HRD (OV-122\_T). The presence of only 1 confirmed BRCA1/2 mutant HRD model is therefore a limit of the study. Further studies will be performed with a higher number of HRD models (BRCA or other HR-related genes mutated models) in order to validate and strengthen the threshold used for HR status definition. However, our study initially only aimed at setting up a powerful tool combining the automatized quantification of RAD51 foci and a method of data processing that could be used for HR scoring in ovarian PDO, rather than validating this tool on a large cohort of patients. Such validation should be performed later in the context of a large and homogeneous cohort of patients receiving platinum-based therapy and PARPi if relevant.

To date, the literature shows that to differentiate HRP from HRD tumor samples, a postirradiation cutoff of 5 RAD51 foci per proliferative cell has been considered informative in the context of manual analysis.<sup>15,16,31</sup> However, in our study, we have shown that as the average number of RAD51 foci exceeds the threshold of 5, this threshold loses its discriminatory capacity. Indeed, our results have been obtained with a high-sensitivity scanner with camera sensors surpassing the resolution of the human eye and allowing more accurate identification of the number of nuclear foci on WSI. Considering this, and as demonstrated by the Gaussian analysis, we proposed the new thresholds of 13 or 16 RAD51 foci per proliferative cell to differentiate cells engaged in XR-induced HR DNA repair from others. However, we have shown that the threshold used has a significant impact on HR classification, making the threshold approach inconclusive or biased. In order to consider the great heterogeneity of PDO profiles over time, we used an approach aiming at making each model its own reference. The creation of 3 new indexes (as described in the result section) and their representation in a PCA space enabled us to distinguish 2 groups of PDO that could be classified as HRD or HRP. Compared with the companion academic test currently used in clinical practice, our classification based on RECAP test was correlated to the genome instability score GIScar.<sup>13</sup> Only 1 model of 10 (OV-122\_T) showed a discrepancy and was classified as HRD by the RECAP test classification and HRP by the GIScar score. The BRCA-mutated only model was classified as HRD by the RECAP test and HRDmid by the GIScar score. Interestingly, compared with the patient's clinical status, RECAP test could allow us to identify HRD tumors that are not captured by the GIScar scoring. Indeed, the patient OV-122 was considered platinum-sensitive with a long PFI (over 20 months). Moreover, it should be noted that the patient tumor was Myriad-positive, and the patient received Olaparib as a first-line maintenance.

The RAD51 assay has also been shown to have some limitations, as previously suggested by Castroviejo-Bermejo et al.,<sup>29</sup> in particular, in the case of HR alterations downstream of RAD51 or those depending on RAD51-independent mechanisms. For example, the ATM protein is also involved in the later steps of HR, particularly after end resection and RAD51 nucleofilament

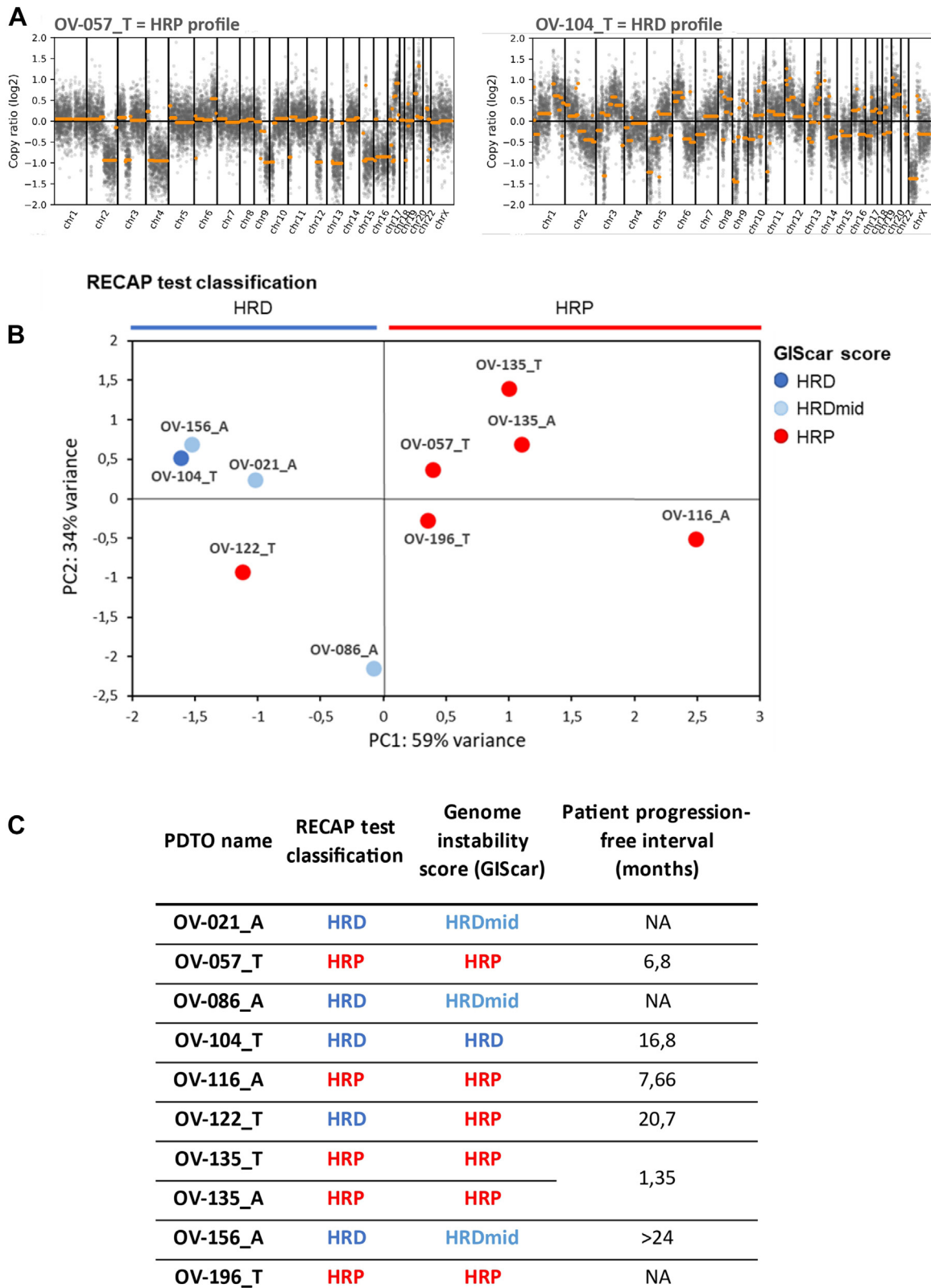


**Figure 4.**

Determination of HR score. (A) Examples of an HR (OV-057\_T) and an HRD (OV-104\_T) profiles determined by the genome instability scoring using the academic test genome instability score (GIScar). (B) PCA using the 3 indexes (basal HR foci index, radio-induced HR foci index and repair index) of the 10 PDTO models. HR classification using the RECAP test results is represented on the top of the PCA and HR classification using the GIScar scoring is represented by a colored dot under each PDTO point. (C) Comparison of the HR status determined by the RECAP test or by the GIScar scoring with the patient platinum-free interval. HRD, homologous recombination deficiency; HRP, homologous recombination proficient; NA, non applicable; PCA, principal component analysis, PDTO, patient-derived tumor organoids; RECAP, repair capacity; XR, X-ray.

formation in the S/G2 phases. When ATM is inhibited, tumor cells exhibit an HRD status, indicating that the RAD51 assay may fail to identify ATM-mutated tumors that would also benefit from PARPi.<sup>32</sup>

Although these results require validation in a larger set of PDTO, other teams also suggest the benefit of establishing organoids from multiple tumor sites in the same patient and assessing HR status in locally advanced or metastatic cancer patients.<sup>33,34</sup> In our study, PDTO derived either from the tumor or ascitic fluids from the same patient (OV-135\_T and A) displayed the same HRP status that was itself correlated to the genomic scoring. This result suggests that ascitic fluids could constitute a relevant material for HR status evaluation that could be of particular interest in the context of a longitudinal evaluation of this status, for instance, to predict the response to PARPi after recurrence when the solid tumor is difficult to obtain. However, other studies have previously demonstrated that carcinomatosis tumor nodes' genomic and transcriptomic features could significantly differ from the primary tumor ones and that this should be considered in the context of personalized treatment.<sup>35-37</sup> Otherwise, it has also been shown that carcinomatosis tumor nodes features were closer to each other than from the primary tumor.<sup>36</sup> However, these studies performed a decade ago did not investigate the HR status variation between the same patient samples, and to our knowledge, no data are yet available about this. Solid tumor sampling bias could thus persist, and the interest in working with ascites versus peritoneal carcinomatosis nodes versus primary tumors remains to be defined. This will be an important point to investigate in the future in order to define the best way to obtain a reliable evaluation of HR status.

In conclusion, we showed that fluorescence immunohistochemistry of Cyclin A2 and RAD51 can be automatically detected and quantified simultaneously, allowing us to go beyond the widely used manual estimation of proteins of interest. Interestingly, this method could easily be applied to other biological materials than PDTO such as FFPE tumors as well as fresh tumor fragments or slices irradiated before paraffin-embedding, which could also be used for clinical investigation of HR status.

The implementation of high-resolution imaging and automated quantification process pave the way for setting a new classification approach, first to identify positive cells for RAD51 foci formation following irradiation and second to conclude about HR status on tumor samples and 3D models. Finally, this new automated tool to score HR status may be used as a complement to NGS-based tests in order to increase the number of patients eligible for PARPi therapies identified through a functional assay. Whether such functional assay could be applied in the context of routine management for patients identified as HRP by genomic analyses remains to be determined by further investigation.

#### Acknowledgments

The authors thank Drs Yannick Saintigny from CNRS/CEA UMR6252 Cimap research Unit (LARIA lab, Caen, France), Elodie Perez, Jérôme Toutain, and Myriam Bernaudin from CNRS UMR6030 ISTCT research Unit (Caen, France) and Hanadi Skeif from University of Caen Normandy, Cyceron platform (Caen, France) who provided scientific advice and technical support. The authors thank Nicolas Goardon and Angelina Legros from SÉSAME facility (Comprehensive Cancer Centre F. Baclesse, Caen, France) who provided technical support for NGS analyses.

#### Author Contributions

L.T., N.E., P-M.M., L-B.W., B.P., and L.P. performed study concept and design. L.T., P-M.M., and R.F. performed PDTO experiments. F.G. performed immunohisto staining. L.T., N.E., and B.P. performed the RECAP test analysis. A.R. and R.L. performed the GIScar analysis. M.B., J-F.L., S.M., and E.D. contributed to the study protocol and collected clinical data. C.B-F. provided anatomopathological expertise. L-B.W., G.B., B.L., F.J., D.V., B.P., and L.P. supervised the experiments. L.T., N.E., P-M.M., L-B.W., B.P., and L.P. wrote the paper. All authors read and approved the final manuscript.

#### Data Availability

The data that support the findings of this study are available from the corresponding authors, upon reasonable request.

#### Funding

Lucie Thorel was funded by a grant from Normandy Regional Council, the University of Caen and the Comprehensive Cancer Center François Baclesse. Pierre-Marie Morice was supported by the Cancer Institut Thématique Multi-Organisme of the French National Alliance for Life and Health Sciences (AVIESAN) Plan Cancer 2014-2019 (doctoral grant). This work is part of "ORGAPRED," "ORGATHEREX," "ONCOTHERA," and "POLARIS" projects, co-funded by the Normandy County Council, the European Union within the framework of the Operational Programme ERDF/ESF 2014-2020, which was conducted as part of the planning contract 2015-2020 between the French State and the Normandy Region. It has also been funded by the Normandy County Council in the framework of Normandy Research program, by the Ligue Contre le Cancer, Calvados Committee, by the Canceropôle Nord-Ouest (Emerging Project Calls), by the Fondation de l'Avenir (#AP-RM-19-020), and by the VAINCRABE association. This study was supported by the HABIONOR European project, co-funded by the Normandy County Council, the French State in the framework of the interregional development Contract CPIER "Vallée de la Seine" 2015-2020.

#### Declaration of Competing Interest

None reported.

#### Ethics Approval and Consent to Participate

Informed consent forms were signed by all patients and were obtained either by the Biological Resources Center "OvaResources," which has received NF 96 900 accreditation (N° 2016/72860.1) or in the context of the "OVAREX" clinical trial (N°ID-RCB: 2018-A02152-53, NCT03831230), in accordance with ethical committee and European law.

#### Supplementary Material

The online version contains supplementary material available at <https://doi.org/10.1016/j.labinv.2025.104097>

#### References

1. Cancer Genome Atlas Research Network. Integrated genomic analyses of ovarian carcinoma. *Nature*. 2011;474(7353):609–615.

2. Li X, Heyer WD. Homologous recombination in DNA repair and DNA damage tolerance. *Cell Res.* 2008;18(1):99–113.
3. Bryant HE, Schultz N, Thomas HD, et al. Specific killing of BRCA2-deficient tumours with inhibitors of poly(ADP-ribose) polymerase. *Nature.* 2005;434(7035):913–917.
4. Farmer H, McCabe N, Lord CJ, et al. Targeting the DNA repair defect in BRCA mutant cells as a therapeutic strategy. *Nature.* 2005;434(7035):917–921.
5. O’Neil NJ, Bailey ML, Hieter P. Synthetic lethality and cancer. *Nat Rev Genet.* 2017;18(10):613–623.
6. Sonnenblick A, de Azambuja E, Azim HA, Piccart M. An update on PARP inhibitors—moving to the adjuvant setting. *Nat Rev Clin Oncol.* 2015;12(1):27–41.
7. González-Martín A, Pothuri B, Vergote I, et al. Niraparib in patients with newly diagnosed advanced ovarian cancer. *New Eng J Med.* 2019;381(25):2391–2402.
8. Ray-Coquard I, Pautier P, Pignata S, et al. Olaparib plus bevacizumab as first-line maintenance in ovarian cancer. *New Engl J Med.* 2019;381(25):2416–2428.
9. Coleman RL, Oza AM, Lorusso D, et al. Rucaparib maintenance treatment for recurrent ovarian carcinoma after response to platinum therapy (ARIEL3): a randomised, double-blind, placebo-controlled, phase 3 trial. *Lancet.* 2017;390(10106):1949–1961.
10. Alexandrov LB, Nik-Zainal S, Wedge DC, et al. Signatures of mutational processes in human cancer. *Nature.* 2013;500(7463):415–421.
11. Hoppe MM, Sundar R, Tan DSP, Jeyasekharan AD. Biomarkers for homologous recombination deficiency in cancer. *J Natl Cancer Inst.* 2018;110(7):704–713.
12. Watkins JA, Irshad S, Grigoriadis A, Tutt ANJ. Genomic scars as biomarkers of homologous recombination deficiency and drug response in breast and ovarian cancers. *Breast Cancer Res.* 2014;16(3):211.
13. Leman R, Muller E, Legros A, et al. Validation of the clinical use of GIScar, an academic-developed genomic instability score predicting sensitivity to maintenance olaparib for ovarian cancer. *Clin Cancer Res.* 2023;29(21):4419–4429.
14. Morice PM, Coquan E, Weiswald LB, Lambert B, Vaur D, Poulain L. Identifying patients eligible for PARP inhibitor treatment: from NGS-based tests to 3D functional assays. *Br J Cancer.* 2021;125(1):7–14.
15. Naipal KAT, Verkaik NS, Ameziane N, et al. Functional ex vivo assay to select homologous recombination-deficient breast tumors for PARP inhibitor treatment. *Clin Cancer Res.* 2014;20(18):4816–4826.
16. Meijer TG, Verkaik NS, Sieuwerts AM, et al. Functional ex vivo assay reveals homologous recombination deficiency in breast cancer beyond BRCA gene defects. *Clin Cancer Res.* 2018;24(24):6277–6287.
17. Kopper O, de Witte CJ, Lohmussaar K, et al. An organoid platform for ovarian cancer captures intra- and inter-patient heterogeneity. *Nat Med.* 2019;25(5):838–849.
18. Talevich E, Shain AH, Botton T, Bastian BC. CNVkit: genome-wide copy number detection and visualization from targeted dna sequencing. *PLoS Computat Biol.* 2016;12(4):e1004873.
19. Bankhead P, Loughrey MB, Fernández JA, et al. QuPath: open-source software for digital pathology image analysis. *Sci Rep.* 2017;7(1):16878.
20. Stringer C, Wang T, Michaelos M, Pachitariu M. Cellpose: a generalist algorithm for cellular segmentation. *Nat Methods.* 2021;18(1):100–106.
21. Schmidt U, Weigert M, Broaddus C, Myers G. Cell detection with star-convex polygons. In: Frangi AF, Schnabel JA, Davatzikos C, Alberola-López C, et al., eds. *Medical Image Computing and Computer-Assisted Intervention – MICCAI 2018.* Springer International Publishing; 2018:265–273.
22. van der Walt S, Schönberger JL, Nunez-Iglesias J, et al. scikit-image: image processing in Python. *PeerJ.* 2014;2:e453.
23. scikit-image 0.18.0.dev0 documentation. skimage v0.18.0.dev0 docs. Accessed September 21, 2020. <https://scikit-image.org/docs/dev/index.html>
24. Xuan G, Zhang W, Chai P. EM algorithms of Gaussian mixture model and hidden Markov model. In: *Proceedings 2001 International Conference on Image Processing (Cat. No.01CH37205).* IEEE; 2001:145–148.
25. Jolliffe IT. Principal component analysis and factor analysis. In: Jolliffe IT, ed. *Principal Component Analysis.* Springer; 1986:115–128.
26. Bonilla B, Hengel SR, Grundy MK, Bernstein KA. RAD51 gene family structure and function. *Annu Rev Genet.* 2020;54:25–46.
27. Ward A, Khanna KK, Wiegman AP. Targeting homologous recombination, new pre-clinical and clinical therapeutic combinations inhibiting RAD51. *Cancer Treat Rev.* 2015;41(1):35–45.
28. Cruz C, Castroviejo-Bermejo M, Gutiérrez-Enríquez S, et al. RAD51 foci as a functional biomarker of homologous recombination repair and PARP inhibitor resistance in germline BRCA-mutated breast cancer. *Ann Oncol.* 2018;29(5):1203–1210.
29. Castroviejo-Bermejo M, Cruz C, Llop-Guevara A, et al. A RAD51 assay feasible in routine tumor samples calls PARP inhibitor response beyond BRCA mutation. *EMBO Mol Med.* 2018;10(12):e9172.
30. Compadre AJ, van Biljon LN, Valentine MC, et al. RAD51 foci as a biomarker predictive of platinum chemotherapy response in ovarian cancer. *Clin Cancer Res.* 2023;29(13):2466–2479.
31. Chopra N, Tovey H, Pearson A, et al. Homologous recombination DNA repair deficiency and PARP inhibition activity in primary triple negative breast cancer. *Nat Commun.* 2020;11(1):2662.
32. Bakr A, Oing C, Köcher S, et al. Involvement of ATM in homologous recombination after end resection and RAD51 nucleofilament formation. *Nucleic Acids Res.* 2015;43(6):3154–3166.
33. Hill SJ, Decker B, Roberts EA, et al. Prediction of DNA repair inhibitor response in short term patient-derived ovarian cancer organoids. *Cancer Discov.* 2018;8(11):1404–1421.
34. Tumiati M, Hietanen S, Hynninen J, et al. A functional homologous recombination assay predicts primary chemotherapy response and long-term survival in ovarian cancer patients. *Clin Cancer Res.* 2018;24(18):4482–4493.
35. Malek JA, Martinez A, Mery E, et al. Gene expression analysis of matched ovarian primary tumors and peritoneal metastasis. *J Transl Med.* 2012;10:121.
36. Hoogstraat M, de Pagter MS, Cirkel GA, et al. Genomic and transcriptomic plasticity in treatment-naïve ovarian cancer. *Genome Res.* 2014;24(2):200–211.
37. Bashashati A, Ha G, Tone A, et al. Distinct evolutionary trajectories of primary high-grade serous ovarian cancers revealed through spatial mutational profiling. *J Pathol.* 2013;231(1):21–34.